Mesoscale Variability in Intact and Ghost Colonies of *Phaeocystis antarctica* in the Ross Sea: Distribution and Abundance

by

Walker O. Smith, Jr.[*]

Virginia Institute of Marine Science, College of William & Mary, Gloucester Pt., VA 23062; email: wos@vims.edu

Dennis J. McGillicuddy, Jr.

Woods Hole Oceanographic Institution, Woods Hole, MA 02543; email: dmcgillicuddy@whoi.edu

Elise B. Olson[1]

Woods Hole Oceanographic Institution, Woods Hole, MA 02543; email: elise.black.olson@gmail.com

Valery Kosnyrev

Woods Hole Oceanographic Institution, Woods Hole, MA 02543; email: vkosnyrev@whoi.edu

Emily E. Peacock

Woods Hole Oceanographic Institution, Woods Hole, MA 02543; email: epeacock@whoi.edu

and

Heidi M. Sosik

Woods Hole Oceanographic Institution, Woods Hole, MA 02543; email: hsosik@whoi.edu

*: Corresponding author

[1]: Now at Department of Earth, Ocean, and Atmospheric Sciences, University of British Columbia, Vancouver, BC V6T 1Z4

Running Head: *Phaeocystis* Ghost Colonies

To be submitted to **Journal of Marine Systems**

January 7, 2016

Abstract

Phaeocystis, a genus with a cosmopolitan distribution and a polymorphic life cycle, was observed during summer in the Ross Sea, Antarctica, where large blooms of this haptophyte regularly occur. The mesoscale vertical and horizontal distributions of colonies of *P. antarctica* were assessed using a towed Video Plankton Recorder (VPR). The mean size of colonies was 1.20 mm, and mean abundances within the three VPR surveys were 4.86, 1.96, and 11.5 mL^{-1}. In addition to the typical spherical, transparent colonies, the VPR quantified an optically dissimilar form of colony that had a distinctive translucent appearance. It also measured the abundance of collapsed colonies, similar to those observed previously from cultures and mesocosms, which we called "ghost colonies". The translucent colonial form had a different distribution than the more common colonial form, and at times was more abundant. Relative to intact colonies, the ghost colonies occurred less frequently, with mean abundances in the three surveys being 0.01, 0.08, and 0.0004 mL^{-1}. Ghost colonies generally were found below the euphotic zone, where they often were in greater abundance than intact colonies. However, the relationship of ghost colonies to intact *P. antarctica* colonies was not direct or consistent, suggesting that the formation of ghost colonies from living colonies and their appearance within the water column were not tightly coupled. Given their relative scarcity and low carbon content, it is unlikely that ghost colonies contribute substantially to vertical flux; however, it is possible that we did not sample periods of major flux events, and as a result minimized the importance of ghost colonies to vertical flux. They do, however, represent a poorly documented feature of polar haptophyte life cycles.

Keywords: *Phaeocystis*; mesoscale; Ross Sea, Antarctica; ghost colonies; carbon

1. Introduction

The genus *Phaeocystis* is found throughout the world's oceans, occurring in the Arctic, Antarctic, upwelling areas, the North Atlantic, and tropical and temperate coastal systems (Lancelot et al., 1998; Schoemann et al., 2005). Some of the species have polymorphic life cycles that include flagellated, solitary cells and spherical colonies, which are comprised of non-flagellated cells embedded in an organic envelope. The colonies are filled with seawater internally, are normally spherical during active growth, and range in diameter from 50 µm to 3 cm. They can form extremely dense blooms in a variety of regions, and are considered to be harmful algal blooms based on their indirect, negative effects to local systems (Schoemann et al., 2005; Blauw et al., 2010; Smith et al., 2014b). The mucopolysaccharide envelope around the colonies is relatively tough (Hamm et al., 1999), and in many regions it can represent a substantial contribution to the total particulate organic carbon (POC) pool.

P. antarctica is a dominant species in the Ross Sea and other Southern Ocean regions (Smith et al., 2014a). In the Ross Sea it typically blooms widely in austral spring and attains maximal biomass in mid- to late December, whereupon its biomass is rapidly reduced in the euphotic zone within days or weeks (Smith et al., 2011). However, significant *P. antarctica* biomass can be found throughout the entire growing season at certain locations (Smith and Jones, 2015). Its appearance in spring is thought to result from its ability to photosynthesize and grow at relatively low photon flux densities (Kropuenske et al., 2009), which are characteristic of spring in the Ross Sea due to relatively deep mixed layer depths and ice cover, both of which restrict irradiance availability. After *Phaeocystis* reaches its biomass maximum, it is thought to sink as intact colonies and/or aggregates (Asper and Smith, 1999, 2003), but also to liberate cells from the envelope into the water column where they develop flagella. Single cells are small (~ 5 µm;

Mathot et al., 2000) and can be preyed upon by microheterotrophs such as dinoflagellates or ciliates. It has been suggested that events of *P. antarctica* sinking in spring are important fluxes to depth and to the sediments (DiTullio et al., 2000), although such events have never been detected by time-series sediment traps. In contrast, Riegstad and Wassmann (2007) proposed that most of the organic matter generated by *Phaeocystis* is remineralized within the water column, especially when contrasted to diatomaceous POC, and that little *Phaeocystis*-derived organic matter was sequestered for long time periods. Verity et al. (1988) also observed forms of colonies that were largely devoid of cells, and called these "ghost colonies". They hypothesized that ghost colonies formed when the individual cells of sinking, senescent (nitrogen limited) colonies were liberated from the mucous envelope, and that the mucoid material sank to depth. Ghost colonies, however, are exceedingly difficult to observe using discrete water samples, given their unknown vertical distribution, translucent appearance, potentially rapid sinking rates and fragile nature. Therefore, their occurrence, distribution and dynamics have never been adequately described.

In recent years the Video Plankton Recorder (VPR) has been developed to observe and quantify the distribution of plankton in the ocean's surface layer (Davis et al., 1996, 2005). Specific forms can be analyzed by pattern recognition algorithms, which automatically identify selected taxa of interest. The advantage of the VPR is that it can sample the upper layer of the ocean at small scales (both vertically and horizontally), allowing the descriptions of plankton distributions within mesoscale and sub-mesoscale features (e.g., Davis and McGillicuddy, 2006; McGillicuddy et al., 2007), as well as jets, eddies and ephemeral plankton patches (Davis et al., 1996).

We deployed a VPR within the ice-free waters of the Ross Sea during austral summer 2012 to assess the mesoscale distributions of plankton and their relationship to iron inputs and water mass structure (McGillicuddy et al., 2015). Summer is a period where *P. antarctica* contributions to biomass are normally decreasing, and diatom contributions increasing (Smith et al., 2014a), although substantial spatial variability in this pattern has been observed (Arrigo et al., 1999; Smith et al., 2013). We hypothesized that *P. antarctica* distributions were correlated with iron fluxes and irradiance levels, and hence would be influenced by mesoscale features throughout the continental shelf and contribute to the substantial spatial variability. As part of our observations, we detected and quantified the distribution and abundance of *P. antarctica* ghost colonies; this report describes the vertical and horizontal distribution of these colonies, their relationship to intact colonies and potential significance in the Ross Sea.

2. Materials and Methods

We conducted VPR tows and sampled the water column as part of the PRISM (Processes Regulating Iron Supply at the Mesoscale) project. Sampling occurred from January 9 through February 6, 2012 from the *R.V.I.B. N.B. Palmer* Cruise NBP12-01. Water samples were collected using a rosette system with 24 10-L Niskin bottles fitted with Teflon-coated external closures. A SeaBird 911+ CTD system, WetLabs fluorometer, BioSpherical quantum sensor, and SeaTech transmissometer were also mounted on the rosette. Samples were collected for discrete chlorophyll *a* analysis (JGOFS, 1996) and particulate organic carbon and nitrogen (Gardner et al., 2000).

A Video Plankton Recorder (Mark II) was towed behind the ship at 10 knots to assess the plankton composition as well as the small-scale hydrographic structure. The VPR was fitted with sensors to measure depth, temperature, salinity, chlorophyll fluorescence and optical backscattering, as well as a digital video camera and strobe, which collected 30 image frames per second. Resolution of the camera system was ca. 10 µm, allowing plankton of ca. 50 µm and larger to be visualized. Individual regions of interest (ROIs) were extracted from each image frame by firmware that detects objects within the field of view, and the ROIs were stored on a computer. Density was calculated from standard relationships among depth, salinity and temperature, and mixed layer depths estimated by a change of 0.01 σ_T units (Thompson and Fine, 2003; Smith et al., 2013). A total of 12 VPR tows were completed, and the lengths of tows ranged from 6 – 36 h. In this analysis we present data from three VPR surveys (Surveys 3, 8 and 9; Fig. 1), in which *P. antarctica* colonies represented a considerable contribution to phytoplankton biomass over at least some of the survey. Surveys 3, 8 and 9 consisted of 46, 212 and 41 complete oscillations from surface to depth, respectively. In addition, the mesoscale variability observed among these three surveys was substantial, and is representative of some of the mesoscale variability that is encountered in the Ross Sea (Fig. 2).

Fluorescence was converted to chlorophyll *a* concentrations by regressing chlorophyll values from CTD casts taken immediately prior to or just after (within 6 h) all VPR transects (using the fluorescence data from the first or last oscillation of the VPR). Calibration locations occurred throughout the entire Ross Sea (Fig. 1). Only those depths where no surface inhibition of fluorescence (FL) was observed were used to obtain the regression. The regression obtained was

$$\text{CHL } (\mu\text{g L}^{-1}) = 0.666\text{FL} + 1.17 \ (R^2 = 0.64; N = 144; p < 0.001)$$

with N being the number of samples and p the significance as determined by a t-test. Optical backscattering data were similarly converted to particulate organic carbon (POC) concentrations by regressing the optical backscattering values (OBS) with all POC concentrations determined from discrete samples. The regression obtained was

$$\text{POC } (\mu\text{mol L}^{-1}) = 512\text{OBS} - 16.9 \ (R^2 = 0.45; N = 129; p < 0.001)$$

All data are available at the Biological and Chemical Oceanography Data Management Office (http://www.bco-dmo.org/project/2155).

Plankton images (ROIs) from the VPR were initially sorted with a dual classifier (Hu and Davis, 2006) trained with ca. 200 examples of each of several morphologies, including individual *P. antarctica* colonies (where there was only one clearly identifiable colony in the image; Fig. 3a), multiple *P. antarctica* colonies (images where colonies were so dense as to create overlap of colonies in the image; Fig. 3b), and ghost colonies (recognizable shapes of colonies that were collapsed, mostly bean-shaped entities; Fig. 3c). Each machine-classified data set was then manually checked to correct both false positives and false negatives for the various *Phaeocystis* categories. Because the classification scheme does not enumerate individual colonies within images of multiple *P. antarctica* colonies, we analyzed 304 images of multiple colony appearance to estimate the average number of colonies (38) contained in images of multiple colonies. To estimate the total number of *P. antarctica* colonies, we summed the number of ROIs with individual colonies and the product of the number of ROIs with multiple colonies and the average number of colonies per multiple-colony ROI (38). Concentrations were calculated by summing abundances in 1-s bins and dividing by the volume sampled (quantified using the tethered copepod method described in Davis et al. 2005).   In addition to counting numbers, the size of colonies was quantified in a subset of the images. Variations in the appearance of colonies were also noted. Some were much more transparent than others (Fig. 3b), while others were more translucent (Fig. 3d). Verity et al. (1987) also noted systematic difference in appearance of colonial forms and attributed these to variations in the life history of colonies. We were unable to verify the stages of the life forms we observed, but have noted the distributions and appearance differences when they occurred.

Lastly, we note that the concentrations of *P. antarctica* were at times so high that the VPR firmware would extract overlapping ROIs of colonies within the field of view, thus potentially leading to overestimation of absolute abundance. To quantify the magnitude of this problem, we first computed the fraction of instances in which more than one ROI containing colonies of *P. antarctica* were acquired at precisely the same time (Table 1). This varied between the three VPR tows, averaging about 20%. A representative subset of the overlapping ROIs was examined, and approximately 30% of the colonies present in those images appeared twice; triplicates were extremely rare. We therefore estimate the magnitude of the double-counting problem to be the product of these two percentages, and thus our abundance estimates may be biased upward by 6% as a result of this issue.

3. Results

Three mesoscale VPR surveys were analyzed: VPR 3, VPR 8, and VPR 9 (Fig. 1). Satellite imagery available in real time facilitated targeting an eddy feature in VPR3 (Fig. 2a). Hydrographic observations showed upward doming of the halocline in the eddy interior, with a positive temperature anomaly in the upper layer (Fig. 4). Variations in the density field are dominated by salinity, with upward doming of the pycnocline mirroring that of the halocline. Mixed layers averaged 26.0 ± 8.6 (N = 93) m within the survey. The VPR fluorometer was set to record a maximum of ~5 µg Chl l^{-1}, and it saturated in the upper 50 m throughout much of the transect, making it impossible to quantify the detailed surface structure of the fluorescence field.

However the saturated layer is notably thicker at eddy center than it is at the periphery. Discrete measurements of chlorophyll within the mixed layer indicated that the mean concentration was 10.7 ± 4.06 μg Chl l^{-1}, approximately 75% greater than estimated from fluorescence (Table 2). POC distributions also show enhanced organic carbon concentrations within the eddy (Table 2). Within the eddy, numbers of colonial *P. antarctica* (spherical in shape, visually transparent) were highest at the base of the euphotic zone (Fig. 5a), vertically coincident with a strong pycnocline (Fig. 4c). Later, strong horizontal maxima occurred near a front ca. 12-25 km into the survey (Fig. 5a), as well as at the end of the survey. Large portions of the transect had very low numbers of colonies. The mean concentration of colonies was 4.86 mL^{-1} (Table 2), but 31% of the 1-s bins contained no colonies (Table 3). Maximum colony abundance was estimated to be 72.7 mL^{-1} at 52 m near the front (Fig. 5a). Numbers of translucent forms were extremely low. Colony size averaged 1.20 ± 0.26 mm (N = 75), and the maximum colony size detected was 2.03 mm. Very few non-spherical shaped colonies (e.g., rotational ellipsoids, cylinders; Mathot et al., 2000) were observed.

Ghost colonies were most abundant at the start of the survey and below the depth of the local maximum in *P. antarctica* colonial abundance (Fig. 5b), but were rare elsewhere in the VPR 3 survey. This suggests that the presence of ghost colonies was related to specific physiological and/or oceanographic conditions. Mean abundance of ghost colonies within the survey was 0.01 (± 0.04) mL^{-1}, and maximum abundance was 0.42 mL^{-1} at 108 m near the beginning of the survey (Table 2, Fig. 4). Ghost colonies were a small percentage of the total (ghost colonies plus intact colonies) colonial forms observed in the survey (averaging 2.9% of all forms throughout the sampled water column; Table 2). When only bins with both ghost colonies and intact colonies were analyzed, ghost colonies formed 35% of all forms (Table 2). The maximum percentage occurred from 100 – 120 m (where ghost colonies were 3.3-fold more abundant than intact colonies; Fig. 6) and reflected both the increase in absolute numbers of ghost colonies with depth and the marked decrease in intact colonies. Approximately 59% of the 1-s bins had *P. antarctica* colonies with no ghost colonies, whereas about 4% had only ghost colonies (Table 3); ca. 5% had both. This information leads to conjecture that the ghost colonies observed at depth resulted from export of a near-surface population in the eddy core.

The VPR 8 Survey sampled a zonal transect 76º 40'S (Fig. 7), spanning an area of low chlorophyll to the west and higher chlorophyll to the east, as evidenced by the MODIS composite for January (not shown). Unfortunately, no cloud-free images are available during the time of the survey, but one approximately ten days earlier provides a sense of the mesoscale variations characteristic of this regime (Fig. 2b). Mixed layer depths averaged 25.2 ± 7.6 m (N=414; range 7.8 to 62.4 m), and the strength of the stratification was less in the central and eastern portions of the transect. Chlorophyll concentrations were maximal at 40 m near 177˚E (~100 km into the transect), but POC levels were greatest at the start of the transect (in the west; Fig. 7e). In situ fluorescence data from the VPR are consistent with the satellite depiction, with higher near-surface values to the east and lower values to the west. The two regimes were separated by a frontal boundary at ca. 177ºE (ca. 78 km from the survey start), driven primarily by variations in salinity (the "eastern front"). Another frontal boundary was located at ca. 174ºE (ca. 20 km from the survey start; the "western front"), where the halocline shoaled toward the west and upper ocean temperature was considerably warmer than the surroundings.

These hydrographic structures appear to have had a substantial impact on the distribution of the various forms of *Phaeocystis*. Colonies were most abundant west of the western front and east of the eastern front; the variant form with translucent colonies was found east of the eastern front with a distinctly bimodal vertical distribution (Fig. 8). Mean abundance of colonies was 1.96 mL^{-1} (Table 2), and 16.6% of the 1-s bins had no colonies at all (Table 3). Maximum abundance was 42.4 mL^{-1}. Ghost colonies were most abundant between the two fronts, also exhibiting bimodal vertical structure (Fig. 8d). Maximum concentrations of ghost colonies reached 0.65 mL^{-1} (Fig. 8d; Table 2). As with VPR 3, ghost colonies were a fraction (maximum of 23.5%) of total colonies (Table 2), but their relative and absolute abundance were substantially greater than in VPR 3. When the bins with both forms present were analyzed, 36% of the colonies were ghost colonies. In contrast, intact colonies were less abundant in VPR 8. The percentage of 1-s bins that had only *P. antarctica* colonies was 19.1% (Table 3), and the percentage of bins that had only ghost colonies was 28.1%. 36.3% of the observations had both intact colonies and ghost colonies, a substantially larger proportion than in VPR 3.

VPR 9 was located close to the Ross Ice Shelf and was designed to cross two eddy-like features that were revealed by satellite imagery (Fig. 2c). The features had cool (ca. -0.5˚C), less saline core with warmer, saltier edges (Fig. 9). These eddy features were approximately 25 km in diameter, and appeared to be have been generated by a frontal instability along the edge of the ice shelf (Li et al., submitted). The more eastern feature had a slightly cooler and less saline core than the western feature. Mixed layer depths were very deep – averaging 68.2 ± 18.5 m over the entire transect (N=81; range 33.7 to 101 m), and 82.3 ± 6.5 m at the western feature's center (15-25 km from the transect start). Both features had exceptionally high concentrations of both intact *P. antarctica* colonies and chlorophyll (Figs. 9, 10), with chlorophyll values reaching nearly 20 $\mu g\ L^{-1}$. The elevated chlorophyll levels were observed not only within the euphotic zone (measured to be ca. 30 m deep) but also throughout the entire mixed layer, leading to exceptionally large integrated values (Smith and Jones, 2015). Maximum chlorophyll concentrations were observed between the two features. POC concentrations were maximal at the western edge of the western feature (outside of the feature; Fig. 9) and showed a markedly different distribution from chlorophyll *a*.

P. antarctica colonies in general were distributed throughout the mixed layer within the western feature, averaging 11.5 ± 8.47 mL^{-1}, and reached a maximum concentration of 39.4 mL^{-1} (Table 2); there appeared to be a modest minimum in the water column near 75 m. Only 10.5% of the 1-s bins within the VPR9 survey contained no *P. antarctica*, which emphasizes the large numbers of colonies found and the exceptional vertical extent of their distribution. Abundances were more than double those found within the VPR 3 survey and nearly six-fold greater than found in VPR 8. Colonies were maximal within the eddies and their abundance was greatly reduced at the flanks (Fig. 10), which were characterized by substantially reduced mixed layer depths (Fig. 9c). Translucent colonies were nearly absent inside the eddy cores, and appeared to be more abundant on the flanks—although their concentrations were generally much less than those of the more transparent form (Figs. 10a,b). Indeed, the two forms had a somewhat inverse distribution, with translucent forms occurring at the eddy's edges where mixed layers were reduced, and occurring above and below the mixed layer. Abundance of ghost colonies was very low relative to other surveys (mean 0.0004 mL^{-1}), reaching a maximum of 0.078 mL^{-1}, and was not correlated with any particular location, although there appeared to be slightly more at the western flank of the eddy (Fig. 10d). No spatial relationship could be discerned between ghost colonies and intact *P. antarctica*, and as in other regions, the ratio of ghost colonies to intact colonies was small (Table 2). Indeed, VPR 9 survey showed the greatest concentrations of intact colonies and the smallest number of ghost colonies. Ghost colonies (without intact colonies) were observed in only 1% of the 1-s bins, and both intact and ghost forms occurred in 0nly 0.61% of the bins.

4. Discussion

Although the existence of mesoscale variability in the Ross Sea has been known for years from satellite imagery and moored instrumentation (e.g., Arrigo and McClain, 1994; Hales and Takahashi, 2004; Smith et al., 2011a), a thorough description of these features and assessment of their oceanographic importance continues to be challenging because of the relative paucity of observations on the requisite space and time scales. For example, it has been suggested that mesoscale eddies provide a source of iron to the euphotic zone of the Ross Sea (Smith et al., 2014) in a manner similar to the nitrogen inputs of eddies in the oligotrophic ocean (McGillicuddy et al., 2007). Such inputs can only be quantified with sampling on appropriate scales. Our study used a novel technology (the VPR) and synoptic hydrographic transects to assess the mesoscale variability within features that were identified by satellite imagery. Information collected on these scales exhibits substantially more variability than that collected using more traditional sampling methods (Kaufman et al., 2014; Jones, 2015).

We were able to quantify the absolute abundance of various morphologies of *P. antarctica* colonies within the mesoscale features. Mean concentrations of colonies varied substantially among eddies (from 1.96 to 11.5 mL^{-1}) as well as within eddies (Figs. 5, 8, 10). This concentration is within the range determined microscopically on *Phaeocystis* blooms in the Ross Sea (Mathot et al., 2000). We also found a unique form that appeared to originate from *P. antarctica* colonies, but with collapsed outer envelope and apparently substantially reduced numbers of cells. We denoted these forms a “ghost colonies”, which have been found in previous studies of other *Phaeocystis* species (Verity et al., 1988). Verity et al. (1988) found that ghost colonies were formed upon the onset of nutrient limitation, and it is tempting to speculate that the ghost colonies we report are linked to physiological stresses induced by iron limitation. Iron concentrations within the regions surveyed were indeed low (from 0.02 – 0.1 nM; McGillicuddy et al., 2015) and below the concentration often considered to be limiting in the Southern Ocean (0.1 nM; Sedwick and DiTullio, 1997). Furthermore, underway surveys showed that photosynthetic capacity (F_v/F_m) was also extremely low during our surveys (averaging 0.17; Ryan-Keough et al., submitted), consistent with the possibility of iron limitation (Behrenfeld et al., 2006). We note, however, the underway data are challenging to interpret due to the variable irradiance conditions the assemblages experience immediately prior to measurement. Moreover, it is likely that nutrient limitation, formation of ghost colonies, and their flux to depth are decoupled in time and space, so it is difficult to infer direct relationships.

The spatial relationship of ghost and intact *P. antarctica* colonies was complex. Distributions within the first part of the VPR 3 survey suggested a source-sink relationship, wherein ghost colonies formed from senescent intact colonies sink faster, thus creating a distinct vertical maximum for each form (Fig. 6). In other areas, however, there was nearly an inverse relationship between the two forms. For example, during VPR 9, where extremely deep mixing was noted and intact colonies occurred in all of the deep mixed layers (and most of the entire survey), ghost colonies were nearly absent throughout, with only a few depths having measureable accumulations (Fig. 10). During the VPR 8 survey, intact colonies were relatively more abundant within the first 80 km and ghost colonies were relatively more common beyond 80 km. A similar relationship was noted in VPR 3 survey after the first 20 km, where intact colonies became more common and ghost colonies were nearly absent. Ghost colonies can be locally important and have impacts on carbon export, although their mean abundance over broader areas may be low. In addition, the relative rarity of ghost colonies makes it difficult to draw unequivocal conclusions about spatial relationships.

Notwithstanding difficulties in interpreting complex spatial patterns, we have reported evidence consistent with the idea that the formation of ghost colonies is linked to physiological stress – likely induced by iron limitation. This prompts questions about possible biogeochemical consequences of ghost colony formation. Vertical separation of intact colonies, which are dependent on irradiance for growth and photosynthesis, and ghost colonies is clearest in the initial part of VPR 3 survey, where the maximum in ghost colony abundance occurred some 70 m below that of intact colonies (Fig. 6). Given this vertical separation, it is tempting to suggest that ghost colonies could be a significant component of vertical flux in areas with large *P. antarctica* blooms. However, various aspects of ghost colonies do not fully support this concept. First, even at their maximum abundance, ghost colonies represent a very small portion of total POC. Based solely on their size and the relationships developed by Mathot et al. (2000), an upper bound on their contribution to POC would be 4.9×10^{-5} μmol C L^{-1}, which is trivial compared to total POC. Even if ghost colonies sink rapidly, their contributions based on the amount of carbon they represent, would likely be insignificant. However, as the spatial variability of the Ross Sea represents a temporal mosaic, it is possible that we simply failed to sample high-flux periods, and hence are under-representing the role of ghost colonies in vertical flux. Additional time series measurements using similar technologies are necessary to resolve this uncertainty.

Additionally, while actively growing colonies of *Phaeocystis* generally have few attached bacteria, Verity et al. (1988) found exceptionally large bacterial numbers on ghost colonies, suggesting that this carbon is likely actively remineralized within the water column. Indeed, while it has been speculated that *Phaeocystis* contributes to export to sediments in the Ross Sea (DiTullio et al., 2000), Riegstad and Wassmann (2007) argued that below the mixed layer *Phaeocystis* carbon is more rapidly remineralized than diatomaceous POC. Riegstad and Wassmann's data are consistent with temporal patterns of POC in the southern Ross Sea (Jones, 2015), where POC flux from the mixed layer was correlated with short-term events (storms) which facilitated chlorophyll flux to depth. Furthermore, the early season POC accumulation (presumably of *Phaeocystis* origin) was observed to sink rapidly, but only a small portion (<3%) of the initial POC reached 100 m, consistent with the rapid remineralization of *P. antarctica* POC. Asper and Smith (unpublished) derived POC concentrations throughout the water column using an in situ camera system, and also found that particles identifiable as *P. antarctica* were remineralized in the upper 300 m of the water column. Our POC estimates do not suggest that maximum ghost colony abundance is correlated with enhanced deep carbon concentrations, but further investigation of the role of *Phaeocystis* in carbon export are needed to resolve its role in vertical carbon fluxes.

5. Conclusions

We demonstrate that substantial mesoscale variability in oceanographic and biological variables occurs in the Ross Sea. While each VPR survey was different, taken together they encapsulated a broad range of features in a variety of environments. The presence of colonies of *P. antarctica*, was extremely variable over spatial scales of kilometers to tens of kilometers and vertical scales of meters to tens of meters. Different forms of colonies were observed, including those that appeared translucent and others that were collapsed. The relationship between intact and ghost colonies was spatially decoupled, although in one location intact colonies exhibited a maximum 70 m above the ghost colony maximum, suggesting that ghost colonies formed from senescing intact colonies and sank rapidly to depth. We speculate that the formation of ghost colonies results from extreme iron limitation. Translucent and transparent colonies had a generally inverse relationship, and appear to be distinct phases within the life cycle of *P. antarctica*. Ghost colonies can be locally important, despite the low abundance found over broader areas. On average, it is unlikely that ghost colonies contribute significantly to vertical flux, but it is also possible that our surveys simply did not capture the full range of flux conditions present in the Ross Sea. Nonetheless, the ubitquous presence of ghost colonies suggests that they are an integral component of the life history of populations of *P antarctica*.

Acknowledgements. This research was supported by grants from the National Science Foundation (ANT-0944254 and ANT-0944165). HMS and EEP acknowledge support of the Gordon and Betty Moore Foundation (Grant #2649) for image informatics development. We especially thank L. Delizo for her help in data analysis, as well as our PRISM colleagues for their assistance at sea. We thank the officers, crew, and technical personnel on board the R/V *Nathaniel B. Palmer* for their outstanding support during our seagoing operations. This is VIMS Contribution number XXXX.

References Cited

Arrigo, K.R., McClain, C.R., 1994. Spring phytoplankton production in the western Ross Sea. Science 266, 261–263.

Arrigo, K.R., Robinson, D., Worthen, D., Dunbar, R., DiTullio, G.R., van Woert, M., Lizotte, M., 1999. Phytoplankton community structure and drawdown of nutrients and CO_2 in the Southern Ocean. Science 283, 365-367.

Asper, V., Smith Jr., W.O., 1999. Particle fluxes during austral spring and summer in the southern Ross Sea (Antarctica). J. Geophys. Res. 104, 5345-5360.

Asper, V., Smith Jr., W.O., 2003. Abundance, distribution and sinking rates of aggregates in the Ross Sea Polynya. Deep-Sea Res. I 50, 131-150.

Behrenfeld, M.J., Worthington, K., Sherrell, R.M., Chavez, F.P., Strutton, P., McPhaden, M., Shea, D.M., 2006. Controls on tropical Pacific Ocean productivity revealed through nutrient stress diagnostics. Nature 442, 1025-1028.

Blauw, A.N., Los, F.J., Huisman, J., Peperzak, L., 2010. Nuisance foam events and *Phaeocystis globosa* blooms in Dutch coastal waters analyzed with fuzzy logic. J. Mar. Systems 83, 115-126.

Davis, C.S., McGillicuddy, D.J., 2006. Transatlantic abundance of the N_2-fixing colonial cyanobacterium *Trichodesmium*. Science 312, 1517-1520.

Davis, C.S., Gallagher, S.M., Marra, M., Stewart, W.K., 1996. Rapid visualization of plankton abundance and taxonomic composition using the Video Plankton Recorder. Deep-Sea Res. II 43, 1947-1970.

Davis, C.S., Thwaites, F.T., Gallagher, S.M., Hu, Q., 2005. A three-axis fast-tow digital video plankton recorder for rapid surveys of plankton taxa and hydrography. Limnol. Oceanogr., Meth. 3, 59-74.

DiTullio, G.R., Grebmeier, J., Arrigo, K.R., Lizotte, M.P., Robinson, D.H., Leventer, A., Barry, J.P., van Woert, M.L., Dunbar, R.B., 2000. Rapid and early export of *Phaeocystis antarctica* blooms in the Ross Sea, Antarctica. Nature 404, 595-598.

Gardner, W.D., Richardson, M.J., Smith Jr., W.O., 2000. Seasonal build-up and loss of POC in the Ross Sea. Deep-Sea Res. II, 47, 3423-3450.

JGOFS, 1996. Protocols for the Joint Global Ocean Flux Study (JGOFS) core measurements. IOC SCOR Report 19. Bergen, Norway.

Jones, R.M., 2015. The influence of short-term events on the biological and hydrographic structure of the southwestern Ross Sea. M.S. Thesis, College of William & Mary, 118 pp.

Hales, B., Takahashi, T., 2004. High-resolution biogeochemical investigation of the Ross Sea, Antarctica, during the AESOPS (US JGOFS) program. Global Biogeochemical Cycles 18(GB3006): doi:10.1029/2003GB002165.

Hamm, C.E., Simson, D.A., Merkel, R., Smetacek, V., 1999. Colonies of *Phaeocystis globosa* are protected by a thin but tough skin. Mar. Ecol. Prog. Ser. 187, 101-111.

Hu, Q., Davis, C., 2006. Accurate automatic quantification of taxa-specific plankton abundance using dual classification with correction. Mar. Ecol. Prog. Ser. 306, 51-61.

Kropuenske, L.R., Mills, M.M., van Dijken, G.L., Bailey, S., Robinson, D.H., Welschmeyer, N.A., Arrigo, K.R. 2009. Photophysiology in two major Southern Ocean phytoplankton taxa: photoprotection in *Phaeocystis antarctica* and *Fragilariopsis cylindrus*. Limnol. Oceanogr.-Meth. 54, 1176-96.

Lancelot, C., Keller, M.D., Rousseau, V., Smith Jr., W.O., Mathot, S., 1998. Autecology of the marine haptophyte *Phaeocystis* sp. In: Anderson, D.M., Cembella, A.D., Hallegraeff, G.M.

(Eds.), Physiological Ecology of Harmful Algal Blooms, NATO ASI Series, Vol. G41, Springer-Verlag, Heidelberg, pp. 211-224.

Mathot, S., Smith Jr., W.O., Carlson, C.A., Garrison, D.L., 2000. Estimate of *Phaeocystis* sp. carbon biomass: methodological problems related to the mucilaginous nature of the colonial matrix. J. Phycol. 36, 1049-1056.

McGillicuddy Jr., D.M., Anderson, L.A., Bates, N.R., Bibby, T., Buesseler, K.O., Carlson, C.A., Davis, C.S., Ewart, C., Falkowski, P.G., Goldthwait, S.A., Hansell, D.A., Jenkins, W.J., Johnson, R., Kosnyrev, V.K., Ledwell, J.R., Li, Q.P., Siegel D.A., Steinberg D.K., 2007. Eddy/wind interactions stimulate extraordinary mid-ocean plankton blooms. Science 316, 1021-1026.

McGillicuddy Jr., D.M., Sedwick, P.N., Dinniman, M.S., Arrigo, K.R., Bibby, T.S., Greenan, B.J.W., Hofmann, E.E., Klinck, J.M., Smith Jr., W.O., Mack, S.L., Marsay, C.M., Sohst, B.M., van Dijken, G., 2015. Iron supply and demand in an Antarctic shelf system. Geophys. Res. Letters 42, doi:10.1002/2015GL065727.

Riegstad, M., Wassmann, P., 2007. Does *Phaeocystis* spp. contribute significantly to vertical export of organic carbon? Biogeochem. 83, 217-234.

Ryan-Keogh, T.J., DeLizo, L.M., Smith Jr., W.O., Sedwick, P.N., McGillicuddy Jr., D.J., Moore, C.M., Bibby, T.S. Temporal progression of photosynthetic strategy by phytoplankton in the Ross Sea, Antarctica. J. Mar. Systems (submitted).

Schoemann, V., Becquevort, S., Stefels, J., Rousseau, V., Lancelot, C., 2005. *Phaeocystis* blooms in the global ocean and their controlling mechanisms: a review. J. Sea Res. 53, 43-66.

Sedwick, P.N., DiTullio, G.R., 1997. Regulation of algal blooms in Antarctic shelf waters by the release of iron from melting sea ice. Geophys. Res. Lett. 24, 2515-2518.

Smith Jr., W.O., Ainley, D.G., Arrigo, K.R., Dinniman, M.S., 2014a. The oceanography and ecology of the Ross Sea. Annu. Rev. Mar. Sci., 6, 469-487.

Smith Jr., W.O., Asper, V., Tozzi, S., Liu, X., Stammerjohn, S.E., 2011. Continuous fluorescence measurements in the Ross Sea, Antarctica: scales of variability. Prog. Oceanogr. 88, 28-45.

Smith Jr., W.O., Jones, R.M., 2015. Vertical mixing, critical depths, and phytoplankton growth in the Ross Sea. ICES J. Mar. Science 72, 1952-1960.

Smith Jr., W.O., Tozzi, S., Sedwick, P.W., DiTullio, G.R., Peloquin, J.A., Long, M., Dunbar, R., Hutchins, D.A., Kolber, Z., 2013. Spatial and temporal variations in variable fluorescence in the Ross Sea (Antarctica): environmental and biological correlates. Deep-Sea Res. I 79, 141-155.

Smith Jr., W.O., Liu, X., Tang, K.W., Delizo, L.M., Doan, N.H., Nguyen, N.L., Wang, X., 2014b. Giantism and its role in the harmful algal bloom species *Phaeocystis globosa*. Deep-Sea Res. II 60, 95-106.

Thompson, R.E., Fine, I.V., 2003. Estimating mixed layer depth from oceanic profile data. J. Atmosph. Ocean. Technol. 20, 319-330.

Verity, P.G., Villareal, T.A., Smayda, T.J., 1988. Ecological investigations of blooms of colonial *Phaeocystis pouchetti*. II. The role of life-cycle phenomena in bloom termination. J. Plankton Res. 10, 749-766.

Table 1. Number of instances in which multiple ROIs containing colonies of *Phaeocystis antarctica* were acquired from the same camera frame ($N_{multiple}$), the total number of *P. antarctica* ROIs (N_{total}), and the percentage of $N_{multiple}$ relative to N_{total}. Note that only a portion of the VPR 8 survey (Figs. 1, 2b) is analyzed here.

Tow ID	$N_{multiple}$	N_{total}	$N_{multiple}$ (%)
VPR3	6,690	38,790	17
VPR8	8,240	48,360	17
VPR9	28,020	113,830	25

Table 2. Mean temperature (20 m), salinity (20 m), chlorophyll *a* and particulate organic carbon concentrations, and intact *Phaeocystis antarctica* (IC) and ghost colony (GC) abundances (all with standard deviations and range encountered). Note that only a portion of the VPR 8 survey (Figs. 1, 2b) is analyzed here.

Property/Survey No.	**VPR 3**	**VPR 8**	**VPR 9**
Temperature (°C)	-0.43 (± 0.28)	0.46 (± 0.49)	-0.52 (± 0.28)
	[-0.89 – 0.27]	[-1.14 – 1.34]	[-0.74 – 0.22]
Salinity	34.04 (± 0.06)	34.32 (± 0.05)	34.13 (± 0.04)
	[33.99 – 34.22]	[34.22 – 34.43]	[34.09 – 34.23]
Mixed layer depth (m)	26.0 (± 8.6)	25.6 (± 7.5)	68.2 (± 18.5)
	[8.6 – 43.7]	[7.8 – 62.4]	[33.7 – 101]
Chlorophyll *a* (µg L^{-1})[1]	6.31 (± 0.71)	4.09 (± 1.84)	7.98 (± 0.86)
	[2.99 – 6.53]	[1.34 – 7.60]	6.18 – 12.3]
Chlorophyll *a* (µg L^{-1})[2]	10.7 (± 4.06)	3.98 (± 1.15)	7.56 (± 2.54)
	[6.18 – 16.7]	[2.51 – 5.89]	[3.74 – 16.0]
Particulate organic	25.2 (± 4.1)	24.8 (± 2.46)	28.7 (± 3.29)
carbon (µmol L^{-1})[3]	[19.4 - 45.5]	[19.4 – 49.1]	[24.5 – 37.8]
Particulate organic	26.6 (± 7.43)	24.6 (± 5.55)	34.9 (± 10.8)
carbon (µmol L^{-1})[2]	[17.4 – 37.2]	[15.7 – 34.1]	[19.3 – 53.8]
P. antarctica colonies	4.86 (± 7.94)	1.96 (± 4.24)	11.5 (± 8.47)
(mL^{-1})[4]	[0.0 – 72.7]	[0.0 – 42.4]	[0 – 39.4]
Ghost colony abundance	0.01 (± 0.04)	0.08 (± 0.10)	0.0004 (± 0.001)
(mL^{-1})[4]	[0.00 – 0.42]	[0.0 – 0.65]	[0 – 0.078]
GC/(GC+IC) (%)[5]	2.85	23.5	0.81
GC/(GC+IC) (%)[6]	35.3	35.9	46.6

[1]: estimated from VPR fluorescence at 20 m
[2]: from discrete samples in mixed layer at stations taken within one day before or after and within the area of the VPR surveys
[3]: estimated from VPR optical backscattering at 20 m
[4]: entire 115 m sampled
[5]: mean of all percentages from entire 115 m sampled, non-zero IC
[6]: mean of all percentages from entire 115 m sampled, non-zero IC, non-zero GC

Table 3. Percentages of 1-s bins in which *Phaeocystis antarctica* colonies and ghost colonies were present in the three VPR surveys. Note that only a portion of the VPR 8 survey (Figs. 1, 2b) is analyzed here.

Property/Survey No.	**VPR 3**	**VPR 8**	**VPR 9**
Number of 1-s bins	10,677	23,093	9,612
Bins with no colonies	31.3	16.6	10.5
Bins with only intact *P. antarctica* colonies (%)	59.1	19.1	87.9
Bins with only *P. antarctica* ghost colonies (%)	4.36	28.1	1.01
Bins with both intact *P. antarctica* colonies and ghost colonies (%)	5.20	36.3	0.61

Figure Legends

Figure 1. Map of the Video Plankton Recorder surveys reported in this analysis. Also included are locations of stations used to calibrate the fluorescence and optical backscattering data. The 500 m depth contour is shown, and the red square in the inset is the PRISM sample area. S and E indicate the locations of the start and end of the VPR surveys. Note that only a portion of the VPR8 survey is reported on here.

Figure 2. MODIS satellite pigment images showing the eddy-like features sampled. A) VPR 3 (8 January, 2012), B) VPR 8 (10 January, 2012), and C) VPR 9 (24 January, 2012). The color bar refers to satellite-derived chlorophyll and is expressed in log chl (µg L^{-1}). The absolute concentrations of pigments measured by satellites and ship sampling differ substantially, but the patterns of the distributions are similar (Li and McGillicuddy, this volume). The black line indicates the VPR track for each survey. Grey represents cloud or ice cover. S and E indicate the locations of the start and end of the VPR surveys. Note that only a portion of the VPR8 survey is reported on here.

Figure 3. Examples of images classified by the automatic counting routine. A) individual *Phaeocystis antarctica* colony; B) multiple *P. antarctica* colonies; C) *P. antarctica* ghost colony; and D) translucent *P. antarctica* colonies.

Figure 4. Distribution during VPR 3 survey of A) temperature (˚C), B) salinity, C) density (σ_T) (kg m^{-3}), D) chlorophyll *a* (µg L^{-1}), and E) particulate organic carbon (µmol L^{-1}). Transect ran from 76.35°S, 175.1°W to 76.55°S, 174.2°W, a distance of 32 km, and then to the north for another 25 km. The turning point is indicated by a dashed line. The fluorometer maximum was 5.0 µg L^{-1} on this survey, but absolute values often exceeded this value as

determined by discrete water sample analyses (Table 2). Here and in Figs. 5, 7-10 the track of the VPR is shown as a dotted blue line.

Figure 5. Distribution during the VPR 3 survey of A) intact *Phaeocystis antarctica* colony abundance (mL^{-1}), and B) ghost colony abundance (mL^{-1}). Transect ran from 76.35°S, 175.1°W to 76.55°S, 174.2°W, a distance of 32 km, and then to the north for another 25 km. The turning point is indicated by a dashed line.

Figure 6. Mean vertical distributions (and standard deviations) of intact *P. antarctica* colony numbers, ghost colonies, and chlorophyll and POC concentrations during the first 12 km of the VPR 3 survey.

Figure 7. Distribution during VPR 8 survey of A) temperature (˚C), B) salinity, C) density (σ_T) (kg m^{-3}), D) chlorophyll *a* (µg L^{-1}), and E) particulate organic carbon (µmol L^{-1}). Transect ran from 76.61°S, 177.9°E to 76.61°S, 179.5°E, a distance of 150 km.

Figure 8. Distribution during the first 125 km of VPR 8 survey of A) "Normal" *Phaeocystis antarctica* colony abundance (numbers mL^{-1}), B) abundance of translucent forms of *P. antarctica* (mL^{-1}), C) total intact *P. antarctica* colony abundance (numbers L^{-1}), and D) ghost colony abundance (mL^{-1}).

Figure 9. Distribution during VPR 9 survey of A) temperature (˚C), B) salinity, C) density (σ_T) (kg m^{-3}), D) chlorophyll *a* (µg L^{-1}), and E) particulate organic carbon (µmol L^{-1}). Transect ran from 77.61°S, 177.93°E to 77.61°S, 179.58°E, a distance of 59 km.

Figure 10. Distribution during the VPR 9 survey of A) "Normal" *Phaeocystis antarctica* colony abundance (numbers mL^{-1}), B) abundance of translucent forms of *P. antarctica* (mL^{-1}), C) total intact *P. antarctica* colony abundance (mL^{-1}), and D) ghost colony abundance (mL^{-1}).

545 Fig. 1

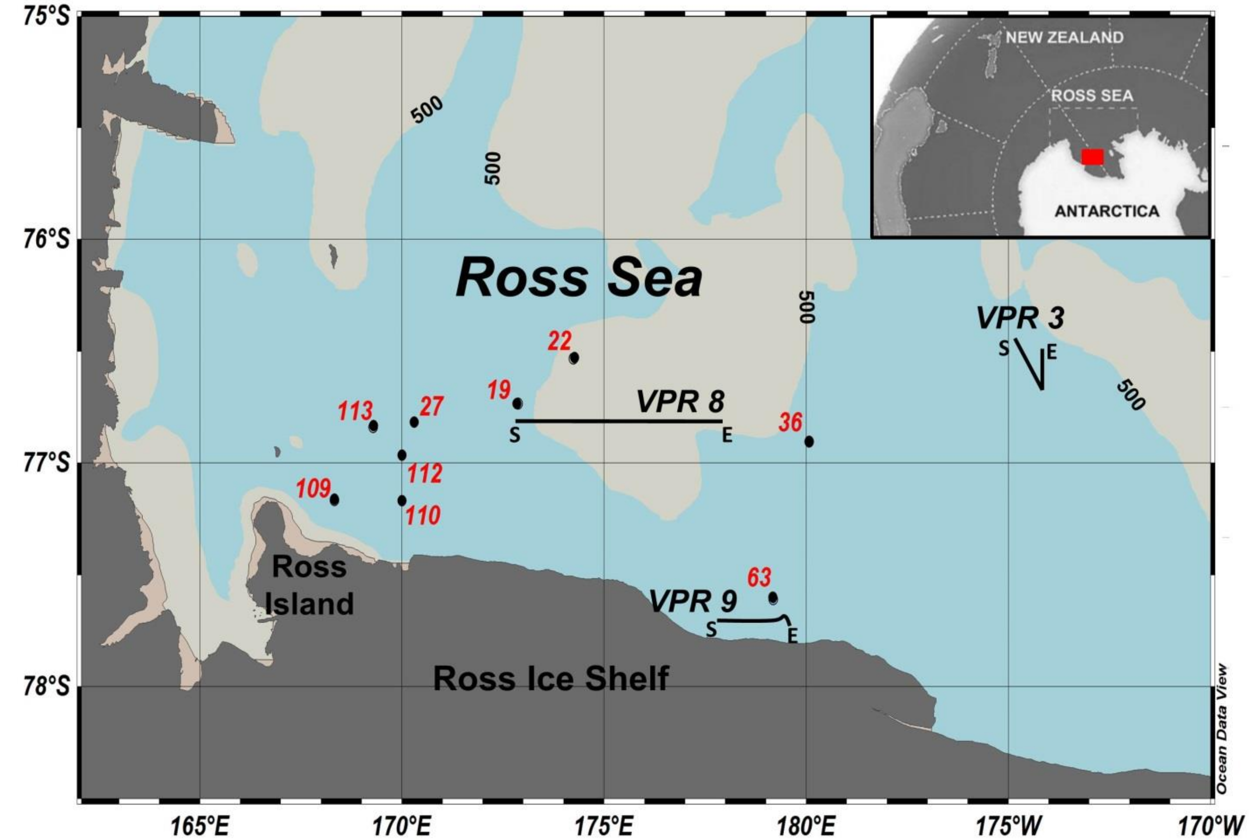
75°S
76°S
77°S
78°S
165°E
170°E
175°E
180°E
175°W
170°W
Ross Sea
500
500
500
500
22
19
113
27
112
109
110
36
63
VPR 8
S
E
VPR 3
S
E
VPR 9
S
E
Ross
Island
Ross Ice Shelf
NEW ZEALAND
ROSS SEA
ANTARCTICA
Ocean Data View

546

Fig. 2. Satellite images

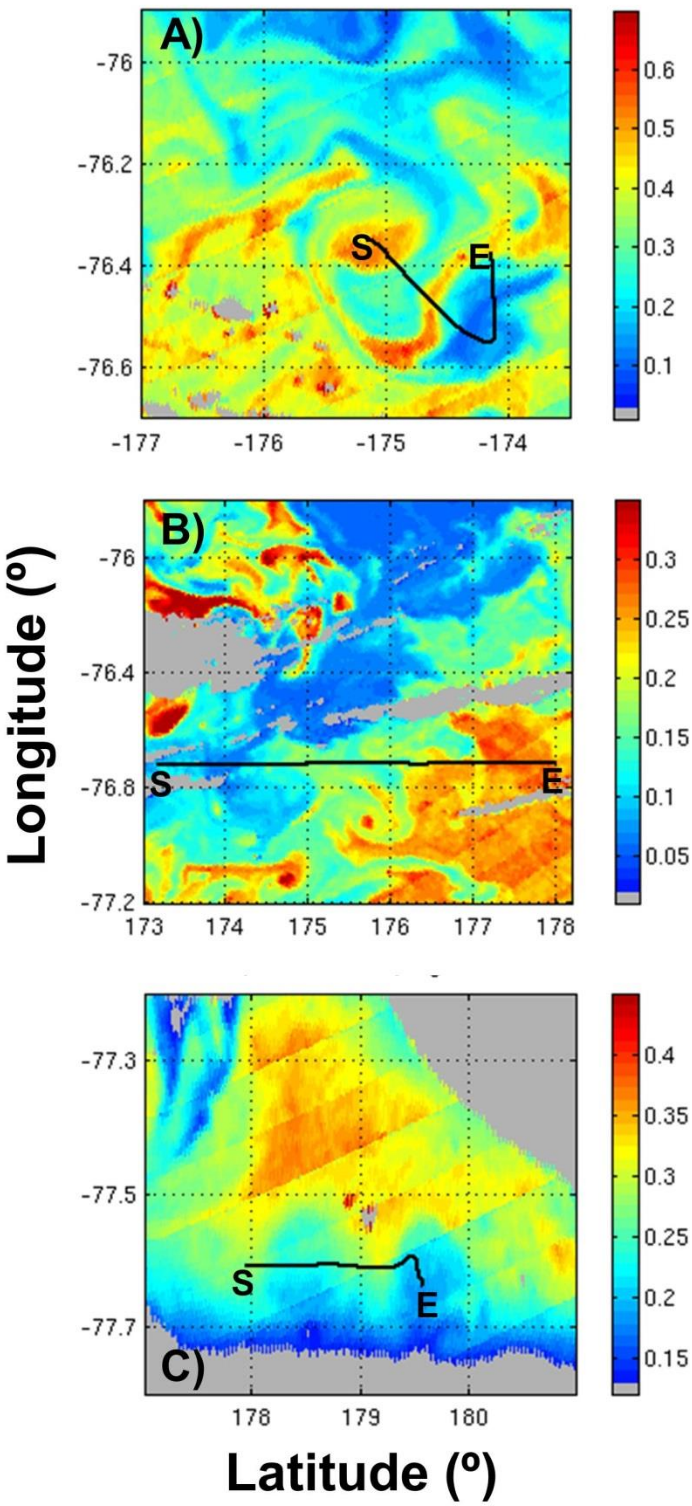

Fig. 3.

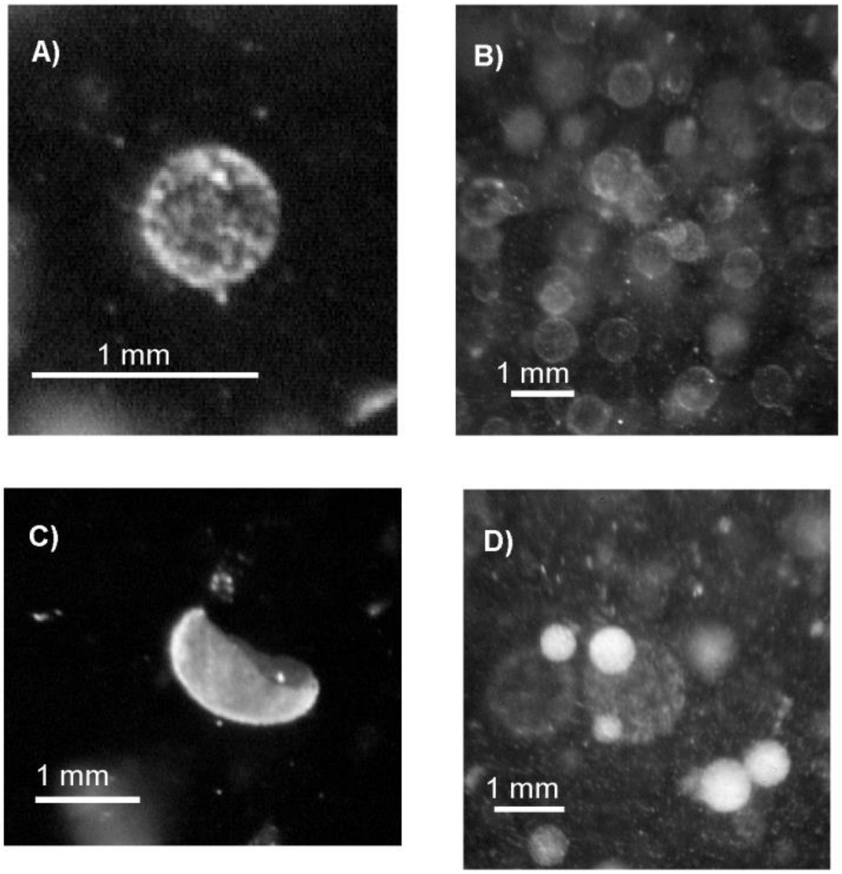

Fig. 4. VPR 3.

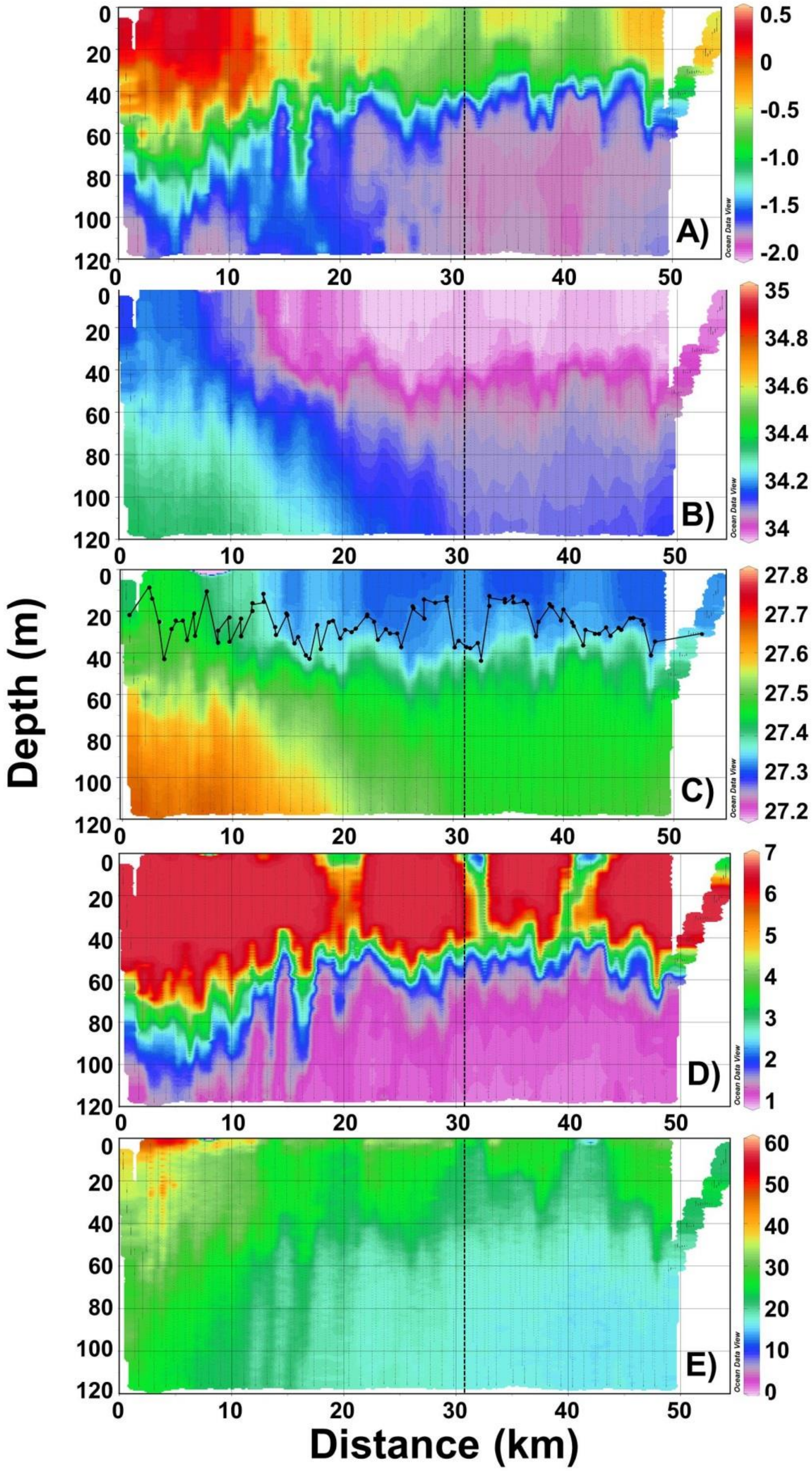
Depth (m)
Distance (km)
A)
B)
C)
D)
E)
0
20
40
60
80
100
120
0
10
20
30
40
50
0.5
0
-0.5
-1.0
-1.5
-2.0
35
34.8
34.6
34.4
34.2
34
27.8
27.7
27.6
27.5
27.4
27.3
27.2
7
6
5
4
3
2
1
60
50
40
30
20
10
0
Ocean Data View

Fig. 5. VPR 3

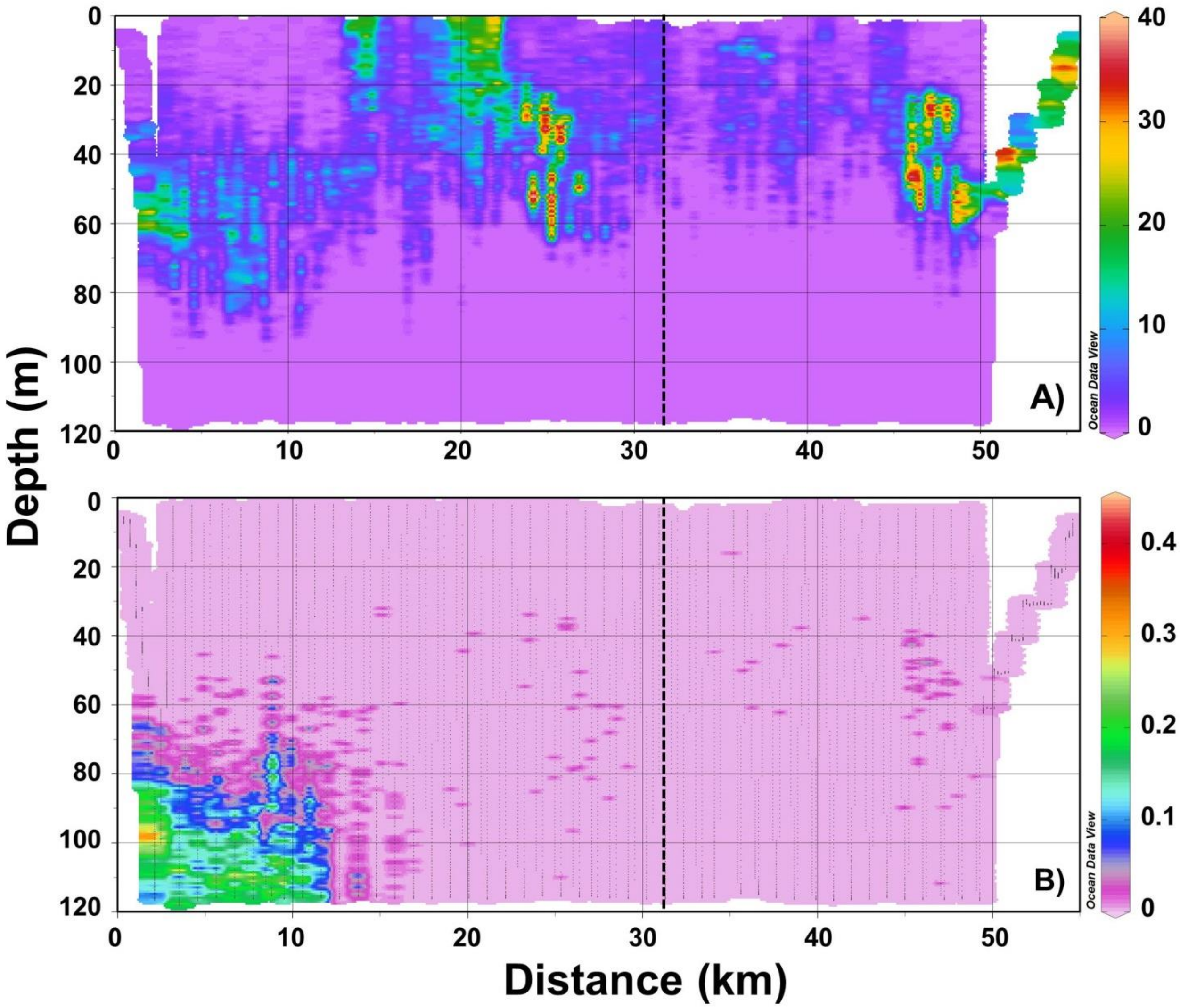
A)
B)
Depth (m)
Distance (km)
Ocean Data View
Ocean Data View
0
20
40
60
80
100
120
0
10
20
30
40
50
0
10
20
30
40
0
0.1
0.2
0.3
0.4

558 Fig. 6.

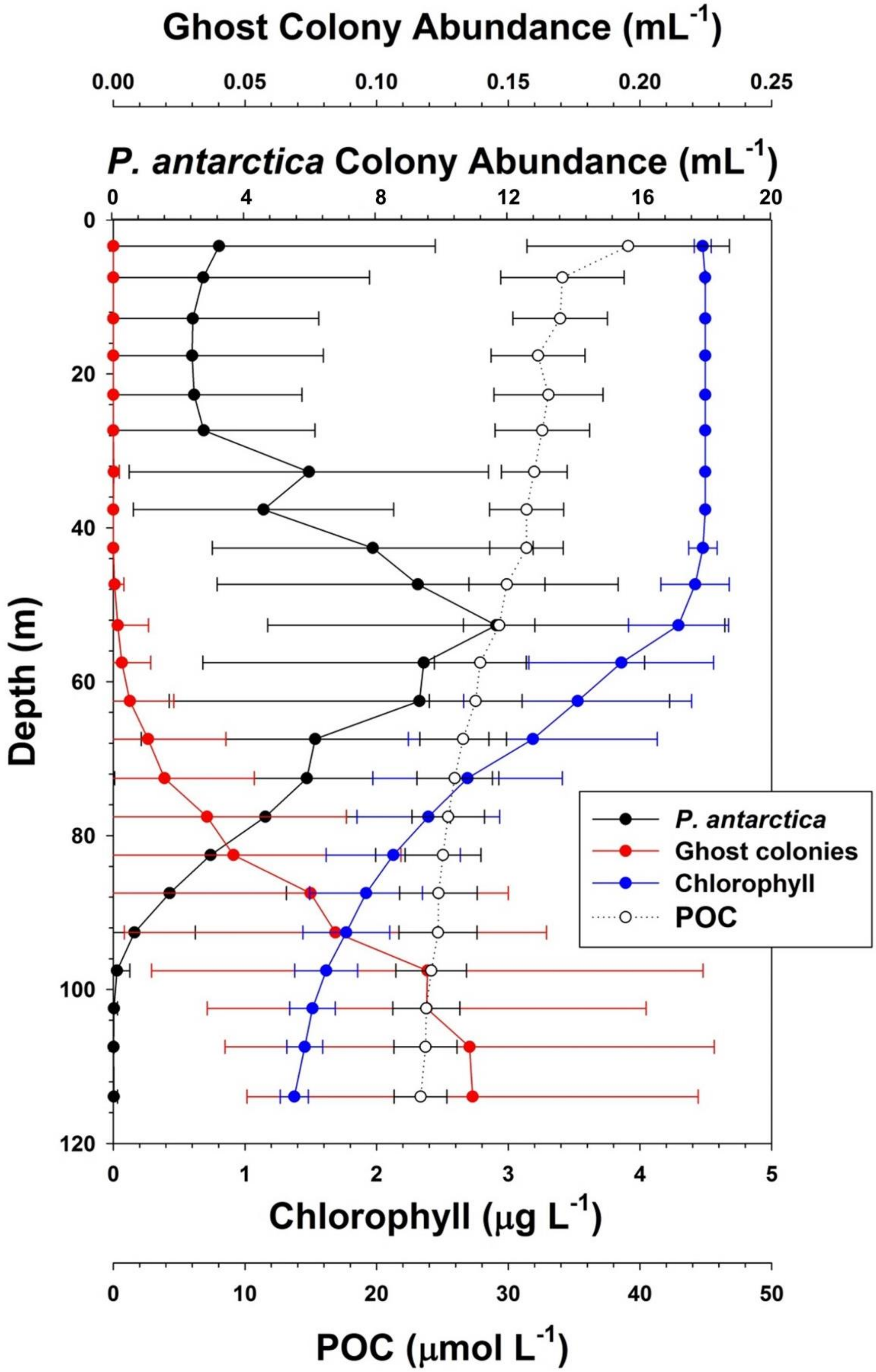

Ghost Colony Abundance (mL-1)
0.00
0.05
0.10
0.15
0.20
0.25
P. antarctica Colony Abundance (mL-1)
0
4
8
12
16
20
Depth (m)
0
20
40
60
80
100
120
P. antarctica
Ghost colonies
Chlorophyll
POC
0
1
2
3
4
5
Chlorophyll (μg L-1)
0
10
20
30
40
50
POC (μmol L-1)

559

Fig. 7. VPR 8

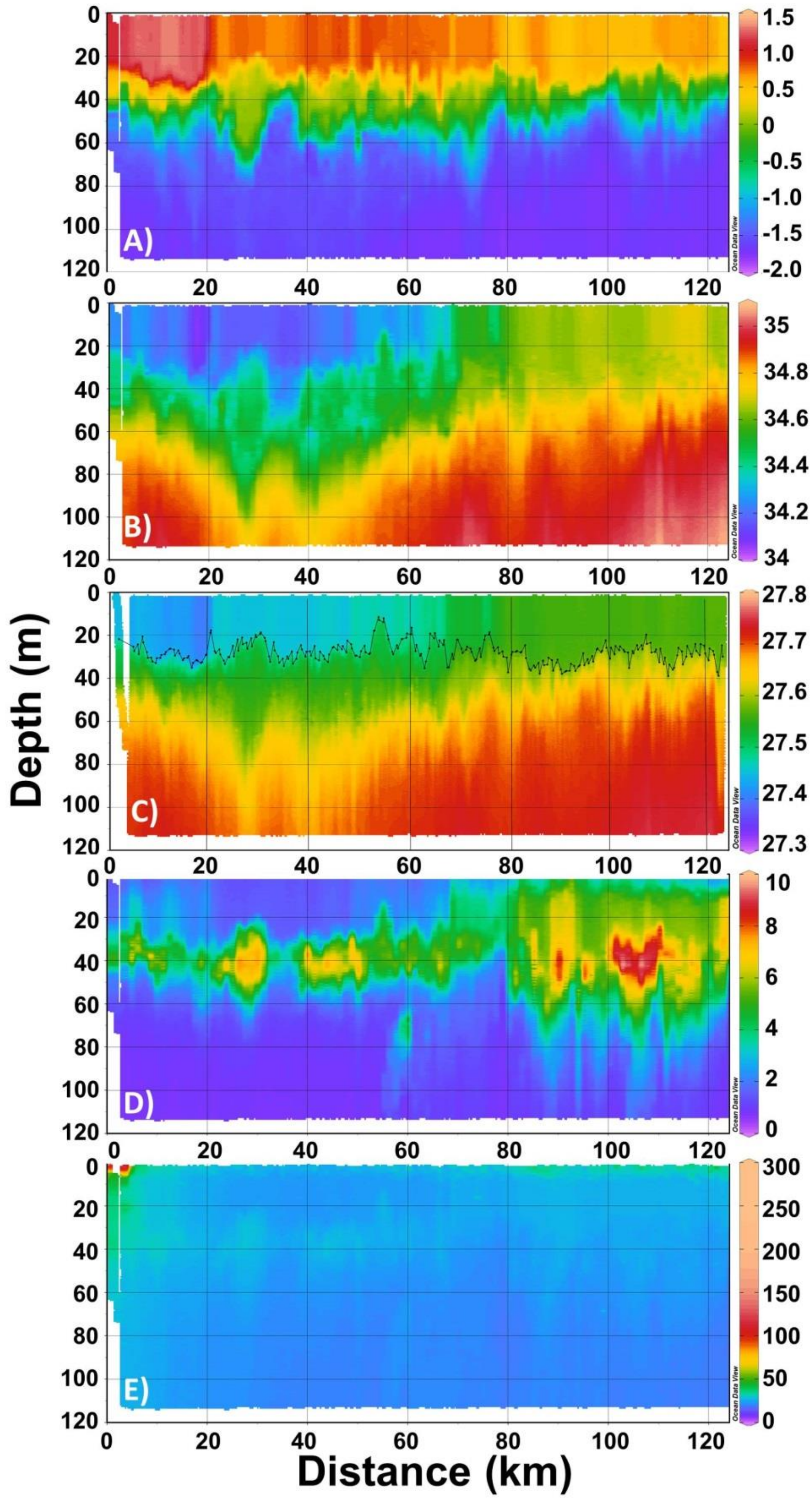
A)
B)
C)
D)
E)
Depth (m)
Distance (km)
0 20 40 60 80 100 120
0 20 40 60 80 100 120
1.5 1.0 0.5 0 -0.5 -1.0 -1.5 -2.0
35 34.8 34.6 34.4 34.2 34
27.8 27.7 27.6 27.5 27.4 27.3
10 8 6 4 2 0
300 250 200 150 100 50 0
Ocean Data View

Fig. 8. VPR 8 colonial data

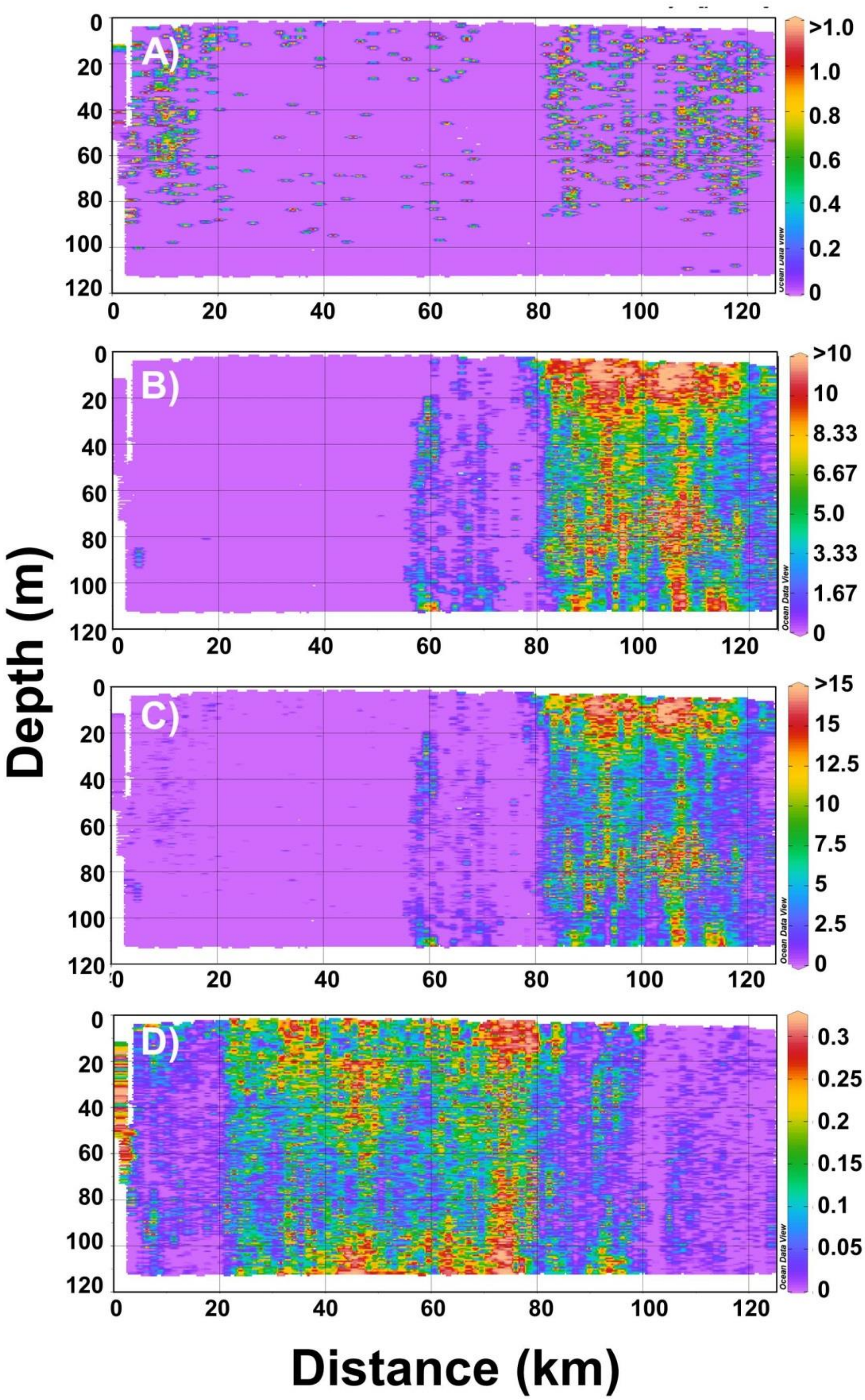

564 Fig. 9. VPR 9 composite.

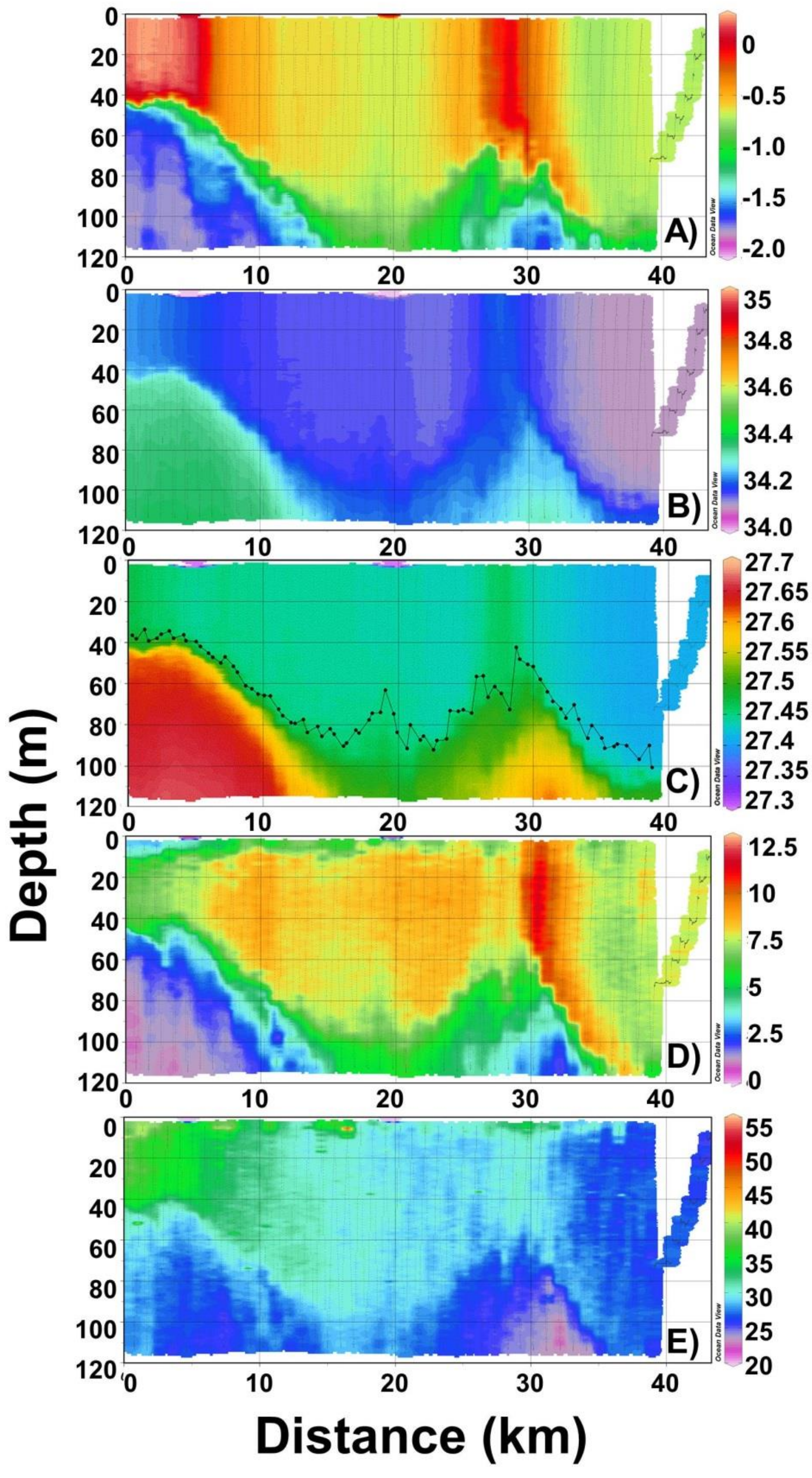

565

Fig. 10. VPR 9

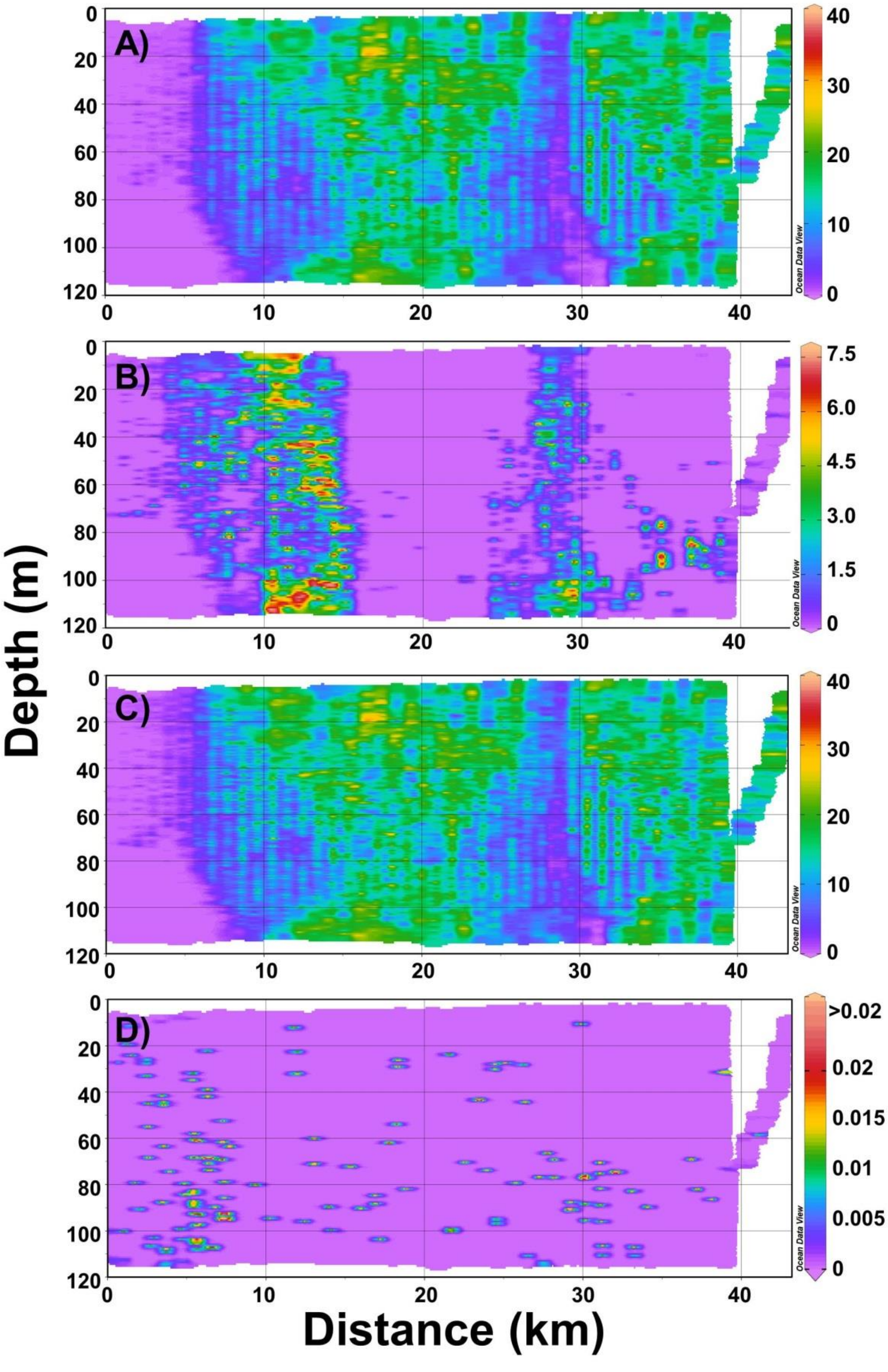
A)
B)
C)
D)
Depth (m)
Distance (km)
0
20
40
60
80
100
120
10
30
40
7.5
6.0
4.5
3.0
1.5
>0.02
0.02
0.015
0.01
0.005
Ocean Data View